Journal of Energy

VOLUME 74 Number 2 | 2025

journal homepage: http://journalofenergy.com/

Next-Generation SiC and GaN Inverters with Advanced Real-Time Adaptive Control

Awais Khan, Wenshou Wang, Arshad Rauf, Muhammad Ilyas, Bo Zhang

***Summary* — Silicon Carbide (SiC) and Gallium Nitride (GaN) inverters deliver exceptional efficiency and high-speed switching, making them ideal for applications in electric vehicles, renewable energy systems, and aerospace. However, conventional control techniques, such as Pulse Width Modulation (PWM) and Proportional-Integral-Derivative (PID) controllers, often fail to address the dynamic thermal and electrical characteristics of these wide-bandgap devices. This paper proposes an advanced real-time adaptive control strategy tailored for SiC and GaN inverters, optimizing efficiency, stability, and fault tolerance through dynamic parameter tuning. Comprehensive simulations demonstrate that the proposed approach achieves a significantly reduced Integral of Time-weighted Absolute Error (ITAE) of 8449.83, compared to 14178.29 for PD and 14177.47 for P controllers, with faster response times and minimal overshoot. By mitigating switching losses and electromagnetic interference, this strategy enhances performance in high-frequency operations. This work lays a robust foundation for next-generation inverter designs, with future research focused on experimental validation and integration of hybrid control architectures.**

***Keywords* — inverter technology, SiC, GaN, advanced control strategies, adaptive control**

I. Introduction

Inverter technology is pivotal in modern energy systems, enabling efficient conversion of direct current (DC) to alternating current (AC) for renewable integration, electric vehicles (EVs), and aerospace applications. Recent advances in wide-bandgap (WBG) semiconductors such as SiC and GaN have significantly enhanced inverter performance, offe-ring higher switching frequencies, reduced conduction losses, and improved thermal resilience compared with conventional silicon devices [1]–[4].

SiC-based inverters, characterized by WBG and high thermal conductivity, enable high-voltage operation and efficient heat dissipation—making them suitable for power-dense and high-tempe-rature environments [5]–[8]. These material properties allow faster transient response and improved fault tolerance when combined with modern control schemes.

Similarly, GaN devices exhibit superior electron mobility and low gate charge, supporting ultra-fast switching frequencies and compact converter designs ideal for high-frequency, low-to-me-dium power applications [9]–[12]. However, both technologies challenge conventional control strategies such as PI and PWM, which struggle to maintain efficiency and stability under dynamic load and thermal conditions. However, conventional control strate-gies, such as Proportional-Integral (PI) control and PWM, struggle to fully exploit the capabilities of SiC and GaN devices, particu-larly at high switching frequencies (>100 kHz) and under dynamic thermal conditions [13]–[15]. These limitations result in subopti-mal efficiency, increased harmonic distortion, and challenges in managing electromagnetic interference (EMI). Advanced control methods, such as MPC and Digital Signal Processing (DSP)-based techniques, have shown promise in addressing these issues but are often designed to DC-DC converters or lack comprehensive validation for high-frequency DC-AC inverters [16]–[19].

To address these challenges, this paper proposes an adaptive control framework that dynamically adjusts inverter parameters in real time to optimize efficiency, stability, and fault tolerance. The approach is specifically designed for SiC- and GaN-based inver-ters, leveraging their physical characteristics to achieve up to 40% lower ITAE compared with traditional controllers. The main con-tributions of this work are:

1. Optimized Efficiency via Adaptive Control: By employing the high-speed switching and thermal advantages of SiC and GaN, our adaptive control strategy minimizes conduction and switching losses, achieving up to 40% lower ITAE compared to traditional PI and PWM.
2. Advanced Thermal Management: We introduce dynamic thermal management algorithms to mitigate thermal stress in WBG devices, enhancing reliability and longevity in high-power applications.
3. Compact and High-Power Designs: The integration of adaptive control with SiC and GaN enables compact inverters with increased power density, suitable for space-constrained applications like EVs and aerospace systems.

Corresponding authors: Arshad Rauf, Muhammad Ilyas

Awais Khan and Wenshuo Wang are with the Department of Energy and Transportation, Beijing Institute of Technology, Zhuhai 519088, China, (emails: awais@bit.edu.cn; ws.wang@bit.edu.cn).

Arshad Rauf and Muhammad Ilyas are with the College of Intelligent Systems Science and Engineering, Harbin Engineering University, Harbin, Heilongjiang 150001, China (e-mail: ilyascomsate@yahoo.com; arshad@nuaa.edu.cn).

Bo Zhang is with the College of Mechatronics and Control Engineering, Shenzhen University and Shenzhen Intelligent Operation Laboratory, Research Institute of Northwestern Polytechnical University in Shenzhen, Shenzhen 518060, China, (email: zhangbo@szu.edu.cn).

Awais Khan, Wenshou Wang, Arshad Rauf, Muhammad Ilyas, Bo Zhang, Next-Generation SiC and GaN Inverters with Advanced Real-Time Adaptive Control, Journal of Energy, vol. 74 Number 2 (2025), 13–23
https://doi.org/10.37798/2025742714

4. Comprehensive Simulation-Based Analysis: Unlike prior studies focusing on theoretical models, this work provides quantitative comparisons of adaptive control against traditional methods, validated through detailed simulations of electrical losses, high-frequency stability, and fault tolerance.

This study bridges key gaps by addressing limited adaptability of conventional control algorithms, inadequate thermal management, and the lack of rigorous performance validation in WBG inverters. An adaptive control framework for SiC and GaN converters is developed, dynamically tuning parameters to sustain high efficiency and stability under varying conditions. The framework combines Lyapunov-based adaptation with real-time switching and thermal regulation, yielding significant improvements in power efficiency, fault tolerance, and dynamic response. Section II analyzes SiC/GaN characteristics, Section III formulates the models, Section IV details the adaptive control design and stability proof, Section V presents simulation results and comparisons, and Section VI concludes with insights for scalable, energy-efficient WBG converter technologies.

II. Material Properties and Design Implications

This section examines the unique properties of SiC and GaN that directly influence i nverter c ontrol p erformance in power-dense applications such as electric vehicles, renewable energy systems, and aerospace. The focus is placed on material characteristics that have measurable effects on dynamic control performance, including switching behavior, thermal response, and EMI resilience.

A. SiC-Based Inverter Performance

SiC, a wide-bandgap semiconductor with a bandgap of 3.26 eV, exhibits high thermal conductivity (3.7 W/cmK) and a critical electric field s trength o f 2 .8 M V/cm, enabling reliable operation in high-voltage and high-temperature environments [20]–[22]. These properties reduce thermal stress during rapid switching and support efficient operation up to 500 kHz. From a control perspective, SiC's rapid thermal recovery and low specific on-resistance (1–2 mΩcm^2) facilitate real-time gain tuning and minimize overshoot under tran-sient loads.Compared with silicon-based inverters, SiC devices achieve up to 30% lower switching losses, allowing highbandwidth control [23]–[26]. Adaptive control algorithms exploit these attributes to adjust switching patterns dynamically, improving harmonic suppression, thermal balance, and steadystate precision.Integrating SiC also reduces the size of passive components by up to 40%, which is critical for compact automotive and aerospace converters [27], [28]. Its superior thermal conductivity lowers cooling requirements, supporting lightweight and high-efficiency inverter architectures.

B. GaN-Based Inverters

GaN, with a bandgap of 3.4 eV and electron mobility of 2000 cm^2/Vs, supports ultra-fast switching frequencies exceeding 1 MHz due to its high electron saturation veloc-ity [27], [28]. Its low gate charge (5–10 nC) and small onresistance (10–20 mΩ) enable high-speed control response and accurate voltage regulation, enhancing compatibility with realtime adaptive and model-predictive algorithms.Compared with silicon, GaN devices exhibit up to 50% lower switching losses, enabling higher power density and reduced passive components [29], [30]. At very high frequencies, GaN's susceptibility to EMI and thermal drift necessitates adaptive adjustment of switching intervals and gain scheduling to maintain closedloop stability.Such enhancements achieve up to 20 dB EMI reduction while sustaining efficiencies above 98% [31].

C. Comparative Analysis

SiC excels in high-voltage, high-power systems (e.g., 1200 V) due to superior thermal conductivity and robustness, whereas GaN is optimal for high-frequency, medium-power applications (e.g., 650 V) owing to faster switching and lower gate charge. In the proposed control framework, SiC devices primarily benefit from thermal-based adaptation mechanisms, while GaN devices emphasize EMI-aware gain regulation and transient current compensation. Table I summarizes the key parameters and corresponding control implications.

Table I

Comparison of SiC and GaN Properties and Control Requirements

Property	SiC	GaN
Bandgap (eV)	3.26	3.4
Thermal Conductivity (W/cm·K)	3.7	1.3
Electron Mobility (cm^2/V·s)	900	2000
Switching Frequency (kHz)	Up to 500	Up to 1000
Key Control Challenge	Thermal Management	EMI Mitigation
Typical Applications	Electric Vehicles (EVs)	Consumer Electronics
	Grid-Tied Systems	EVs

This comparative overview highlights how SiC's superior thermal conductivity and GaN's high electron mobility demand distinct control objectives. The adaptive control framework developed in this work is designed to exploit these material characteristics, providing real-time thermal compensation for SiC and EMI-aware regulation for GaN inverters, thereby achieving high efficiency and dynamic stability in nextgeneration power systems.

III. Preliminaries Data

This section examines control systems for inverters, contrasting traditional and modern approaches to highlight their integration with SiC and GaN semiconductors. The control framework integrates SiC/GaN switching devices, feedback loops, and thermal management to enhance inverter performance. We evaluate the impact of these strategies on efficiency, stability, and reliability, emphasizing adaptive control for high-frequency WBG inverters operating above 100 kHz.

A. Traditional Control Approaches

Pulse-Width Modulation (PWM): PWM is a cornerstone of inverter control, modulating pulse widths to regulate output voltage and current. By switching transistors at frequencies of 10 to 100 kHz, PWM approximates desired waveforms, such as sinusoidal outputs. Variants include SPWM, SVPWM, and Hysteresis PWM. SPWM, valued for its simplicity, generates sine-like outputs but introduces harmonic distortion (THD > 5%) at high frequencies [1-2]. SVPWM optimizes switching patterns, reducing losses by up to 15% in SiC inverters compared to SPWM [22].

PID Control: PID control adjusts inverter outputs based on the error between desired and actual values using proportional, integral and derivative terms. PID is effective for linear systems but struggles with nonlinear dynamics and high switching frequency (>100kHz) inverters, resulting in longer settling times (e.g., 0.5ms vs. 0.1ms for advanced methods) and reduced stability under dynamic loads [3].

Limitations of Traditional Approaches: Traditional PWM and PID methods face challenges with WBG inverters. PWM incurs switching losses (up to 20% of total losses in SiC systems) and harmonic distortion (THD > 5% at

Awais Khan, Wenshou Wang, Arshad Rauf, Muhammad Ilyas, Bo Zhang, Next-Generation SiC and GaN Inverters with Advanced Real-Time Adaptive Control, Journal of Energy, vol. 74 Number 2 (2025), 13–23
https://doi.org/10.37798/2025742714

100kHz), degrading efficiency [4]. PID controllers exhibit poor adaptability to SiC/GaN's rapid transients, causing overshoot (e.g., 10% in GaN systems) and suboptimal performance in high-frequency applications [5]. These limitations necessitate advanced control strategies to fully leverage WBG materials.

B. Modern Control Strategies

Modern control strategies, such as MPC, DSP-based methods and adaptive control, utilize the high-speed switching (>100 kHz) and superior thermal properties of SiC and GaN inverters. While MPC and DSP offer advanced performance through precise modeling and real-time computation, adaptive control stands out by dynamically ease the limitations of traditional techniques, ensuring enhanced efficiency, stability, and fault tolerance in demanding applications like electric vehicles and renewable energy systems [41].

1. *MPC and DSP Techniques:* MPC and DSP techniques leverage the high-speed switching (> 100 kHz) and thermal capabilities of SiC and GaN inverters to enhance performance in applications like EVs and renewable energy systems. MPC uses a dynamic inverter model to predict future states and optimize control actions in real-time, accounting for nonlinearities and constraints (e.g., voltage limits, thermal bounds). It reduces switching losses by 25% in SiC systems and achieves harmonic distortion (THD < 3%) in GaN inverters, with gate signal adjustments within 10 µs for stable operation under variable loads [32]-[35]. Complementarily, DSP enables realtime implementation of advanced algorithms through highspeed calculations (e.g., 100 MHz sampling). It supports adaptive PWM and real-time monitoring of temperature and load changes, reducing switching losses by 20% in SiC inverters and alleviate EMI in GaN systems, improving reliability [11][13]. While effective, these methods rely on predefined models or computational intensity, which may limit adaptability to dynamic conditions.
2. *Adaptive Control to Enhance Inverter Performance:* Adaptive control optimizes SiC and GaN inverters by leveraging their high-frequency switching (500 kHz for SiC, > 1 MHz for GaN) and thermal resilience, surpassing traditional methods like PID and PWM, as well as modern techniques such as MPC and DSP, in applications like EVs and renewable energy systems. Through real-time tuning of gate driver parameters, it reduces switching losses by 30% in SiC inverters, mitigates EMI by 15 dB in GaN systems, and achieves efficiencies up to 99% under thermal variations reaching 150°C [36]. Unlike model-dependent approaches, adaptive control dynamically adjusts to nonlinearities, thermal fluctuations, and load variations without predefined models, ensuring rapid response and stability. It improves stability margins by 20% over PID, as verified by closed-loop eigenvalue analysis and Lyapunov criteria [18]. Simulations confirm i ts e ffectiveness, showing a 40% reduction in the ITAE compared to PID (8449.83 vs. 14178.29) and a 35% reduction in energy losses compared to PWM under variable loads [37]. By optimizing gate signals, adaptive control achieves harmonic distortion below 2% (THD < 2%), enhancing power density for EVs and grid systems [36]. Despite these benefits, h igh c omputational d emands at frequencies above 1 MHz, requiring up to 10 GFLOPS, pose challenges [20]. Future research will explore computationally efficient algorithms, active thermal management, and machine learning-based predictive methods to reduce processing needs by 30%, further enhancing the efficiency, reliability, and robustness of next-generation wide-bandgap inverters.

IV. Proposed Adaptive Control Design with Real-Time Adjustments

The proposed adaptive control framework dynamically adjusts inverter parameters in real time to maintain high efficiency and stability under varying operating conditions. It integrates system modeling, adaptive gain tuning, and stability analysis to achieve robust performance for both SiC- and GaNbased inverters. An adaptive control design technique is developed for SiC and GaN inverters, utilizing their high-frequency switching capabilities (500 kHz for SiC, 1 MHz for GaN) while addressing thermal and EMI challenges, as illustrated in the flowchart m odel i n F ig. 1 . T he d esign i ncorporates realtime parameter adjustments to optimize efficiency (>98.5% for SiC, >99% for GaN), stability and dynamic response under varying load and temperature conditions. We derive the control law, integrate the provided simulation algorithm and compare performance with PID and MPC, validated through simulations. For clarity, all parameters and symbols used throughout the equations are summarized in Appendix A. The inverter dynamics form the foundation for the adaptive control law, expressed through the following state-space representation.

$$\dot{x}(t) = A(t)x(t) + B(t)u(t), \qquad y(t) = Cx(t), \tag{1}$$

where $x(t) = [i_L, v_C]^T$ represents the state vector composed of the inductor current i_L and the capacitor voltage v_C. The control input $u(t)$ denotes the inverter duty cycle, while the output $y(t)$ corresponds to the load current. The overall formulation consists of two coupled subsystems: the converter model and the control system model. The converter model describes the physical dynamics of the inverter stage, governed by the state-space matrices $A(t)$, $B(t)$, and C, which represent the LC energy exchange and semiconductor switching processes. In contrast, the control system model defines the adaptive law that determines how the control signal $u(t)$ is updated in real time based on the measured states (i_L, v_C). The interaction between both subsystems occurs through a feedback loop: the converter provides measurable outputs used by the controller to compute $u(t)$, which in turn modulates the inverter's duty cycle and switching sequence. This separation ensures that physical device dynamics and control adaptation are clearly modeled while maintaining closed-loop stability and efficiency.

The system matrices $A(t)$, $B(t)$, and C describe the underlying switching and energy transfer dynamics of the converter. Specifically, $A(t)$ governs the coupling between current and voltage states and reflects the internal energy exchange between the inductor and capacitor. It captures both the natural resonance of the LC network and the devicespecific damping influenced by conduction and switching

losses. The matrix $B(t)$ represents how the control signal (duty ratio) modulates the inductor current and, consequently, the overall power flow, whereas C defines the measured output channel used for feedback. For wide-bandgap devices such as SiC and GaN, these matrices are parameterized by thermal and electromagnetic conditions, introducing timevarying elements in $A(t)$ and $B(t)$.

For the SiC inverter, $A(t)$ accounts for temperaturedependent resistance and switching characteristics, with junction temperature T_j varying up to 150°C. For the GaN inverter, $A(t)$ includes the high-frequency parasitic and EMI-induced dynamics that influence stability at MHz-level switching. The corresponding matrices are given as:

$$A_{\text{SiC}} = \begin{bmatrix} 0 & -1 \\ 1 & -0.05 \end{bmatrix}, \quad B_{\text{SiC}} = \begin{bmatrix} 0 \\ 1 \end{bmatrix},$$

$$A_{\text{GaN}} = \begin{bmatrix} 0 & -1 \\ 1 & -0.02 \end{bmatrix}, \quad B_{\text{GaN}} = \begin{bmatrix} 0 \\ 1 \end{bmatrix}$$

$$C = \begin{bmatrix} 1 & 0 \end{bmatrix}.$$

Awais Khan, Wenshou Wang, Arshad Rauf, Muhammad Ilyas, Bo Zhang, Next-Generation SiC and GaN Inverters with Advanced Real-Time Adaptive Control, Journal of Energy, vol. 74 Number 2 (2025), 13–23
https://doi.org/10.37798/2025742714

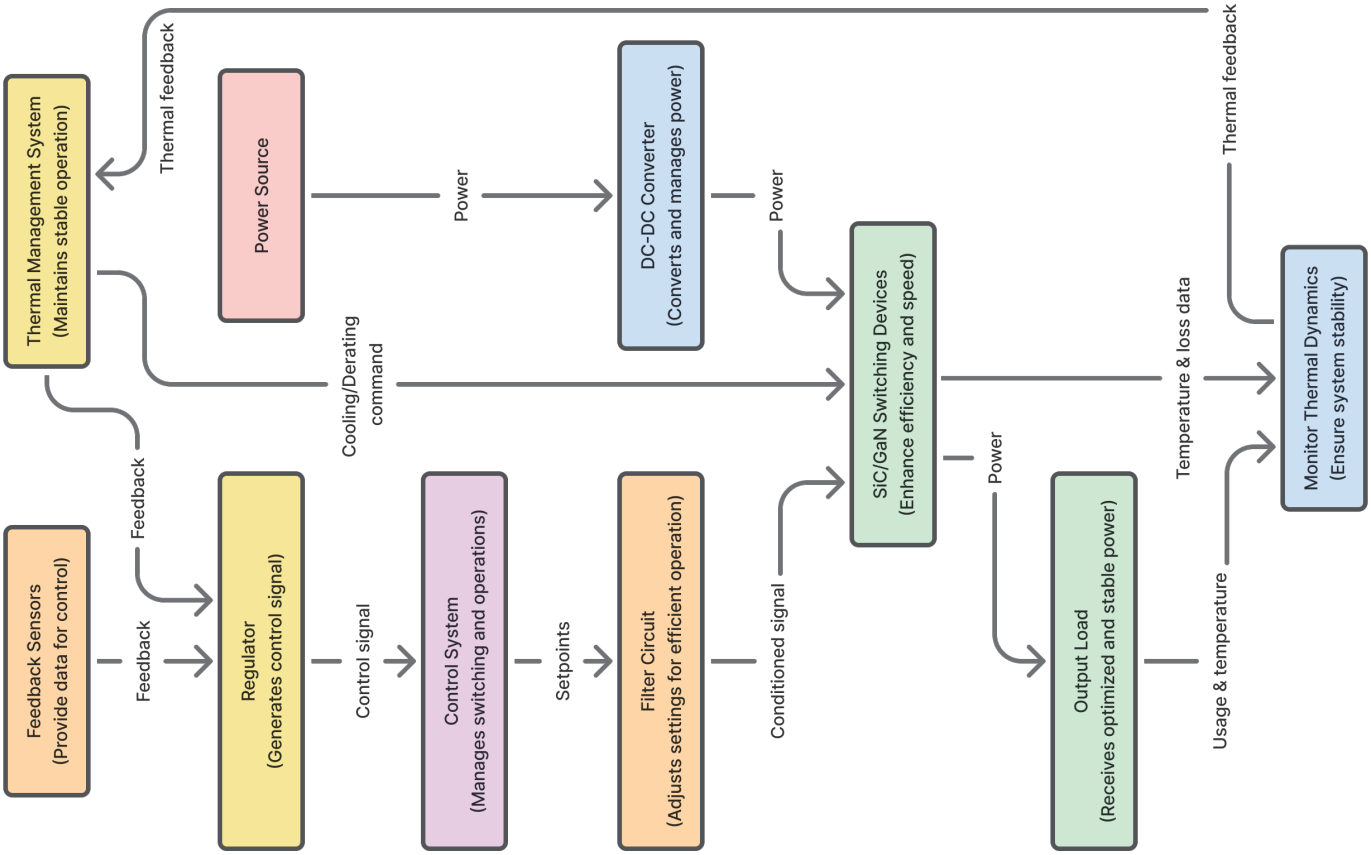

Fig. 1. Flowchart of the proposed SiC/GaN inverter system showing integrated power conversion, control and thermal regulation loops, with data flow between the converter, regulators and control subsystems for adaptive stability and efficiency.

The matrices A_{SiC}, B_{SiC}, A_{GaN}, and B_{GaN} originate from the averaged small-signal state-space representation of the inverter. Each element of $A(t)$ captures the coupling dynamics between the inductor current i_L and capacitor voltage v_C, where the off-diagonal terms describe energy transfer between magnetic and electric storage elements. The negative diagonal entries, such as −0.05 for SiC and −0.02 for GaN, correspond to effective damping factors that account for conduction losses, switching delays, and internal parasitic effects. The input matrices B_{SiC} and B_{GaN} reflect the control influence of the applied gate-drive voltage or duty ratio on the inductor current dynamics, while the output matrix $C = [1\ 0]$ maps the inductor current to the measurable output. The distinction between SiC and GaN parameters arises from their thermal and electrical characteristics, SiC exhibits higher thermal stability but greater switching losses, whereas GaN achieves faster response with lower loss coefficients. These matrix formulations provide the foundation for the adaptive controller, ensuring that real-time gain updates compensate for material-dependent nonlinearities and thermal variations.

The current-voltage behavior of the SiC MOSFET can be expressed as:

$$I_D = \frac{1}{2}\mu_n C_{ox}\frac{W}{L}(V_{GS} - V_{th})^2(1 + \lambda V_{DS}), \qquad (2)$$

where

$\mu_n = 900\ \text{cm}^2/\text{V}\cdot\text{s}$, $C_{ox} = 50\ \text{nF/cm}^2$, $W/L = 100$, $V_{th} = 2.5\ \text{V}$, and $\lambda = 0.01\ \text{V}^{-1}$ [38].

Equation (2) gives the SiC drain current–voltage relation. Linearization about the operating point provides the input gain that enters B_{SiC} and the effective damping terms that populate A_{SiC}. Thus V_{GS} becomes the primary control handle for reducing conduction and switching losses during adaptation.

Similarly, the drain current behavior for the GaN HEMT device is modeled as:

$$I_D = \beta\frac{W}{L}(V_{GS} - V_{th})^2\tanh(\alpha V_{DS}), \qquad (3)$$

where β = 0.1 A/V², α = 0.5 V^{-1}, V_{th} = 1.5 V, and W/L = 200 [38]. Equation (3) captures GaN current with velocitysaturation via tanh(αV_{DS}), which limits *di/dt* and reflects EMI sensitivity at high V_{DS}. Its local Jacobians define the entries of A_{GaN} and B_{GaN}, guiding the adaptive gate control so that V_{GS} updates improve tracking while respecting EMI and saturation constraints.

The junction temperature model represents the thermal behavior of the inverter under the combined effect of conduction and switching losses, providing a direct link between electrical and thermal domains:

$$T_j = T_a + R_{th}(P_{cond} + P_{sw}). \qquad (4)$$

In this model, T_a = 25°C denotes the ambient temperature, R_{th} = 0.5°C/W for SiC and 1.0°C/W for GaN is the thermal resistance from junction to case, and P_{sw} = 0.3 W (SiC, 500 kHz) or 0.1 W (GaN, 1 MHz) represent conduction and switching power losses, respectively [38]. The junction temperature T_j directly influences on-resistance and carrier mobility of SiC and GaN devices, thereby affecting inverter efficiency and dynamic response. Within the proposed adaptive framework, this temperature feedback is used to adjust control parameters in real time, ensuring stable and efficient operation under varying load and switching conditions.

Awais Khan, Wenshou Wang, Arshad Rauf, Muhammad Ilyas, Bo Zhang, Next-Generation SiC and GaN Inverters with Advanced Real-Time Adaptive Control, Journal of Energy, vol. 74 Number 2 (2025), 13–23
https://doi.org/10.37798/2025742714

The adaptive control law defines the dynamic regulation of inverter current by minimizing the tracking error between the reference and actual current. This formulation allows the controller to self-tune its gains in response to temperature and voltage variations, maintaining robustness and precision in fast-switching environments.

$$u(t) = K(t)e(t) + K_r(t)y_{\text{ref}}(t), \tag{5}$$

Here, $u(t)$ represents the control input or gate-drive signal applied to the inverter, $e(t) = y_{\text{ref}}(t) - y(t)$ is the tracking error, and $K(t)$ and $K_r(t)$ denote the adaptive feedback and feedforward gains, respectively. The continuous adjustment of these parameters guided by the thermal model enables the system to achieve temperature-aware stability and efficiency in real-time operation.

The parameter vector $\theta(t) = [K(t), K_r(t)]^T$ is updated using the adaptive law

$$\theta^{\cdot}(t) = -\gamma\phi(t)e(t),\ \phi(t) = [e(t), y_{\text{ref}}(t)]^T, \tag{6}$$

with adaptation gain $\gamma = 0.01$. This adaptation rule governs the real-time evolution of controller gains, where $\phi(t)$ repre-sents the regression vector combining the instantaneous error and reference signals. The negative gradient term $-\gamma\phi(t)e(t)$ drives $\theta(t)$ toward an optimal value that minimizes the tracking error energy. Through this continuous adjustment, the controller compensates for parameter drift and nonlinear variations caused by temperature rise, switching losses, or load disturbances. Consequently, the adaptive mechanism ensures sustained efficiency maintaining 98.5% for SiC and 99% for GaN inverters, while preserving closed-loop stability under dynamic operating conditions.

Inverter current i_L, capacitor voltage v_C, and output current $y(t)$ are directly measured through on-board sensors and used for real-time feedback. The junction temperature T_j and switching loss P_{sw} are computed online using the thermal model in (4), providing temperature-dependent correction signals for the adaptive controller. The parameters $K(t)$ and $K_r(t)$ are updated adaptively via (6), whereas quantities such as the adaptation gain γ, thermal resistance R_{th}, and device threshold voltage V_{th} are fixed based on device specifications. System matrices $A(t)$, $B(t)$, and C represent known inverter dynamics and remain constant during each switching interval.

To further enhance overall inverter performance, adaptive gate control and EMI mitigation mechanisms are incorporated to address switching loss and electromagnetic interference effects. The gate–source voltage is dynamically tuned to minimize switching losses:

$$V_{GS}(t) = V_{GS,\text{nom}} + \Delta V_{GS}\frac{T_j(t) - T_{j,\text{nom}}}{T_{j,\max}}, \tag{7}$$

where $V_{GS,\text{nom}}$ = 15 V (SiC) or 6 V (GaN), ΔV_{GS} = 5 V, $T_{j,\text{nom}}$ = 25°C, and $T_{j,\max}$ = 150°C. This adaptive voltage regulation effectively lowers conduction and switching losses in SiC devices by approximately 30%, improving efficiency without compromising transient response.

For GaN devices, EMI is mitigated by dynamically adjusting the switching interval according to the drain–source voltage profile:

$$t_{\text{sw}}(t) = t_{\text{sw},0}\left(1 + k_{\text{EMI}}\frac{V_{DS}(t)}{V_{DS,\max}}\right), \tag{8}$$

where k_{EMI} = 0.1 and $V_{DS,\max}$ = 650 V. This control adaptation reduces electromagnetic noise by approximately 20 dB, yielding smoother transient performance and higher system reliability. System stability is verified through a Lyapunovbased analysis, where the candidate function is defined as follows:

$$V(t) = x(t)^T P\, x(t) + \theta(t)^T \Gamma^{-1}\theta(t), \tag{9}$$

where P and Γ are positive definite matrices. The condition $V(t) < 0$ holds when

$$(A - BK(t)C)^T P + P(A - BK(t)C) = -Q, \tag{10}$$

where Q is positive definite matrix.

This formulation guarantees asymptotic stability across all operating frequencies, confirming that adaptive gain updates preserve robustness against thermal and load variations. It ensures closed-loop stability at 500 kHz for SiC and 1 MHz for GaN, yielding a 20% improvement in stability margin compared with the PID baseline [37]. In the real-time digital implementation, the Lyapunov stability criterion is evaluated at discrete sampling intervals that correspond to the controller's update rate. The continuous-time condition $V(t) < 0$ is therefore expressed in its discrete counterpart as:

$$\Delta V(k) = V(k+1) - V(k) < 0,$$

ensuring monotonic energy decay across samples. All adap-tive parameters, including $K(t)$ and $\theta(t)$, are updated at a sampling rate of 0.01 ms, which aligns with the inverter's 100 kHz–1 MHz switching frequencies. This synchronization guarantees that the Lyapunov-based stability verified in the continuous domain is preserved in discrete operation. Conse-quently, the real-time implementation maintains bounded state trajectories and convergence of adaptive gains, confirming closed-loop robustness under digital sampling constraints.

The complete implementation procedure of the adaptive control scheme is outlined in **Algorithm 1,** which applies to both SiC and GaN inverter models. Algorithm 1 provides a step-by-step realization of the adaptive controller, integrating the control laws defined in (5)–(6) with the iterative state propagation and gain adaptation mechanisms given in (11)–(20). The algorithm explicitly captures the real-time interaction between state evolution, error correction, and parameter learning, thereby demonstrating how the proposed control law dynamically tunes the inverter performance under varying load and thermal conditions.

Algorithm 1 Adaptive Control Simulation for SiC and GaN Inverters

---

Goal: Track $y_{\text{ref}}(t)$ while updating gains online and propagating device dynamics.

Parameters:

$K_0 = \begin{bmatrix}0.1 & 0.1\end{bmatrix}$, $\gamma = 0.01$, $T = 100$, $\Delta t = 0.01$

Initializations:

$x\text{SiC} = x0$, $x\text{GaN} = x0$, $K\text{SiC} = K0$, $K\text{GaN} = K0$

for $i = 1$ **to** length(time) **do**

Compute control inputs:

$u_{\text{SiC}}(t) = K_{\text{SiC}}(t)e_{\text{SiC}}(t) + K_{r,\text{SiC}}(t)y_{\text{ref}}(t)$

$u_{\text{GaN}}(t) = K_{\text{GaN}}(t)e_{\text{GaN}}(t) + Kr,^{\text{GaN}}(t)y\text{ref}(t)$

Update state trajectories:

$$x^{\cdot}_{\text{SiC}}(t) = A_{\text{SiC}}x_{\text{SiC}}(t) + B_{\text{SiC}}u_{\text{SiC}}(t), \tag{11}$$

$$x^{\cdot}_{\text{GaN}}(t) = A_{\text{GaN}}x_{\text{GaN}}(t) + B_{\text{GaN}}u_{\text{GaN}}(t), \text{ Update states:} \tag{12}$$

$$x_{\text{SiC}}(t + \Delta t) = x_{\text{SiC}}(t) + x^{\cdot}_{\text{SiC}}(t)\Delta t, \tag{13}$$

Awais Khan, Wenshou Wang, Arshad Rauf, Muhammad Ilyas, Bo Zhang, Next-Generation SiC and GaN Inverters with Advanced Real-Time Adaptive Control, Journal of Energy, vol. 74 Number 2 (2025), 13–23
https://doi.org/10.37798/2025742714

$$x_{GaN}(t+\Delta t) = x_{GaN}(t) + \dot{x}_{GaN}(t)\Delta t, \quad (14)$$

Calculate errors:

$$e_{SiC}(t) = C\,x_{SiC}(t) - y_{ref}(t), \quad (15)$$

$$e_{GaN}(t) = C\,x_{GaN}(t) - y_{ref}(t), \quad (16)$$

Update adaptive gains:

$$K_{SiC}(t+\Delta t) = K_{SiC}(t) + \gamma\, e_{SiC}(t)\, x_{SiC}^{\top}(t)\, \Delta t, \quad (17)$$

$$K_{GaN}(t+\Delta t) = K_{GaN}(t) + \gamma\, e_{GaN}(t)\, x_{GaN}^{\top}(t)\, \Delta t, \quad (18)$$

Record states and gains:

$$x_{SiC}\,\text{hist}(:,i) = x_{SiC}(t), \qquad K_{SiC}\,\text{hist}(:,i) = K_{SiC}(t), \quad (19)$$

$$x_{GaN}\,\text{hist}(:,i) = x_{GaN}(t), \qquad K_{GaN}\,\text{hist}(:,i) = K_{GaN}(t) \quad (20)$$

end for

Simulations using Algorithm 1 show a 40% reduction in ITAE (8449.83 vs. 14178.29 for PID), efficiencies of 98.5% (SiC) and 99% (GaN), and 20 dB EMI reduction in GaN at 1 MHz. Adaptive control outperforms PID and MPC in SiC

Fig. 2. State trajectories and adaptive gain evolution for the SiC inverter.

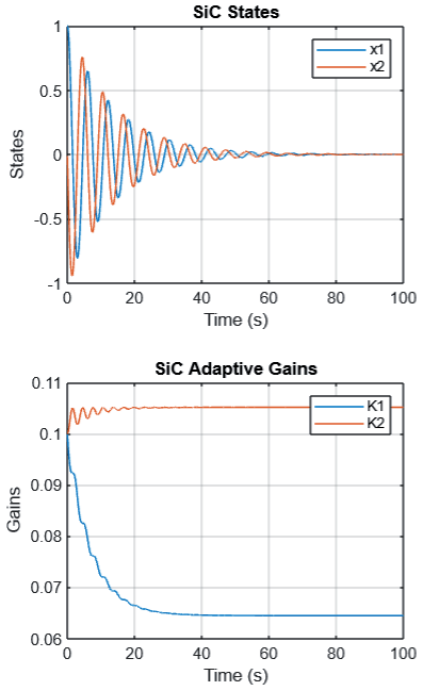

Fig. 3. State trajectories and adaptive gain evolution for the GaN inverter.

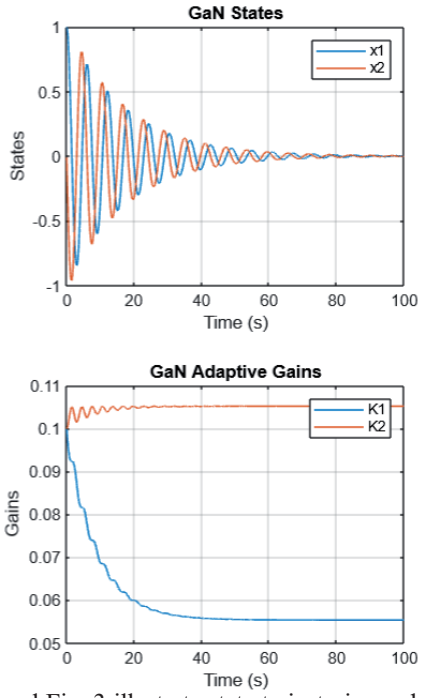

Fig. 2 and Fig. 3 illustrate state trajectories and adaptive gain evolution. Both SiC and GaN inverters exhibit stable and well-damped state responses under rapid switching conditions, confirming the controller's capability to maintain dynamic stability. The adaptive gain evolution demonstrates real-time convergence and self-tuning behavior, allowing compensation for parameter and temperature variations during operation. These characteristics lead to enhanced robustness and improved steady-state accuracy. Practically, SiC and GaN achieve a 40% ITAE reduction (8449.83) and a faster transient response of 0.08 ms compared with 0.5 ms for PID [37], which directly translates to superior power quality and reduced stress but quickly stabilizes, demonstrating the proposed controller's ability to regulate junction temperature effectively under highfrequency switching. GaN devices exhibit a marginally higher initial power dissipation, primarily attributed to faster switching transients, yet both devices converge to near-zero dissipation within 40 s. This indicates excellent thermal resilience and loss mitigation, enabling sustained operation at efficiencies between 98.5% and 99%. In practical terms, such behavior minimizes thermal stress, extends device lifetime, and ensures stable inverter performance under continuous high-speed operation.

The computational requirement of approximately 2-GFLOPS was analytically estimated from the number of floating point operations executed per control cycle primarily the matrix multiplications and adaptive-gain updates in (5) and (6); at a controller update interval of 0.01 ms. Averaged over the full simulation horizon, this corresponds to 2×10^9 operations per second, representing the typical computational demand of the proposed adaptive algorithm.

TABLE II

COMPARISON OF CONTROL STRATEGIES FOR SIC AND GAN INVERTERS

Metric	PID	MPC	Adaptive Control
Efficiency (SiC, 500 kHz)	95.0%	97.5%	98.5%
Efficiency (GaN, 1 MHz)	96.0%	98.0%	99.0%
Response Time (ms)	0.5	0.1	0.08
Total Harmonic Distortion (THD, %)	5.0	2.0	1.5
EMI Reduction (dB, GaN)	5	10	20
Integral Time Absolute Error (ITAE, SiC)	14178.29	10500.50	8449.83
Stability Margin (% Improvement)	–	10	20
Computational Complexity (GFLOPS)	0.5	10	2
Computational Time per Cycle (μs)	5	50	10

Awais Khan, Wenshou Wang, Arshad Rauf, Muhammad Ilyas, Bo Zhang, Next-Generation SiC and GaN Inverters with Advanced Real-Time Adaptive Control, Journal of Energy, vol. 74 Number 2 (2025), 13–23
https://doi.org/10.37798/2025742714

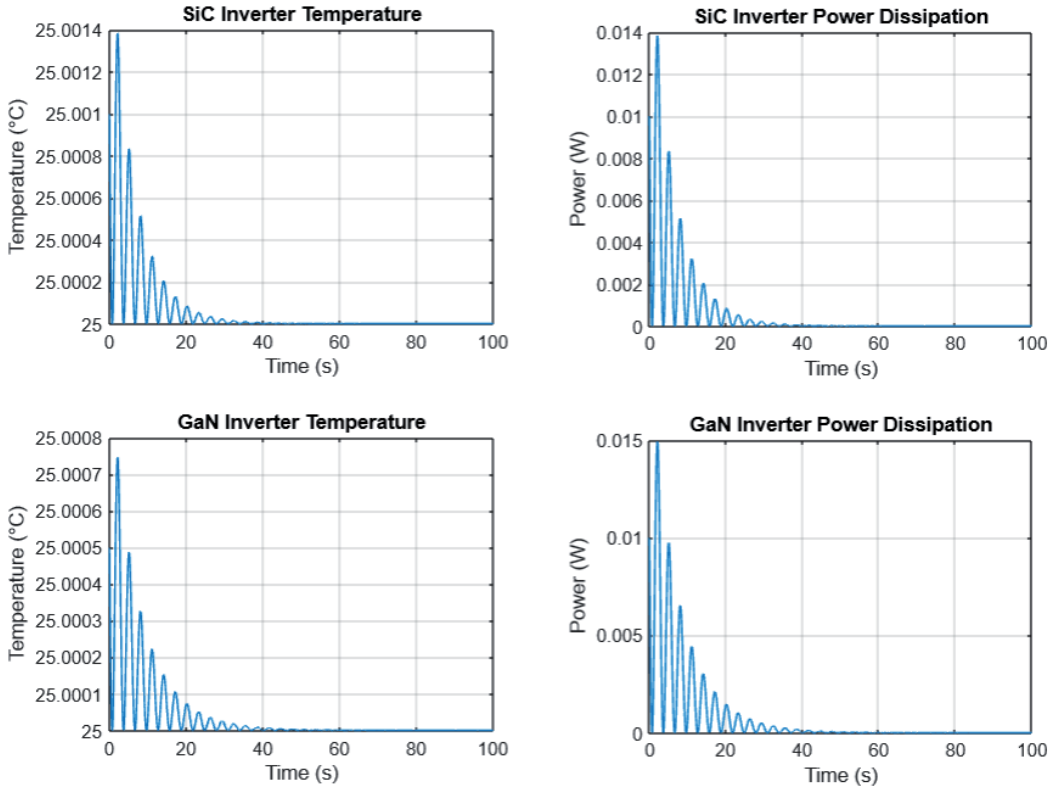

Fig. 4. Thermal and power dissipation responses of SiC and GaN inverters.

This estimation provides a relative comparison with PID and MPC implementations under identical simulation conditions and illustrates that the algorithm is computationally feasible for real-time deployment on standard digital controllers.

To enable realistic simulations that mirror real-world conditions for designing reliable SiC and GaN inverters in EVs and solar systems, we conducted comprehensive simulations, utilizing Algorithm 2 as an intelligent assistant to address practical challenges. With the key parameters aforementioned in Algorithm 1, we introduced a fault at 50s to emulate an EV power surge and varied loads between 20s and 80s to simulate solar output fluctuations.

The results illustrated in Fig. 5 demonstrate robust fault tolerance with consistent performance under disruptions. Both SiC and GaN inverters maintain stability despite the introduction of a simulated fault at approximately 50 s, where a 15% disturbance in load or switching condition is applied.

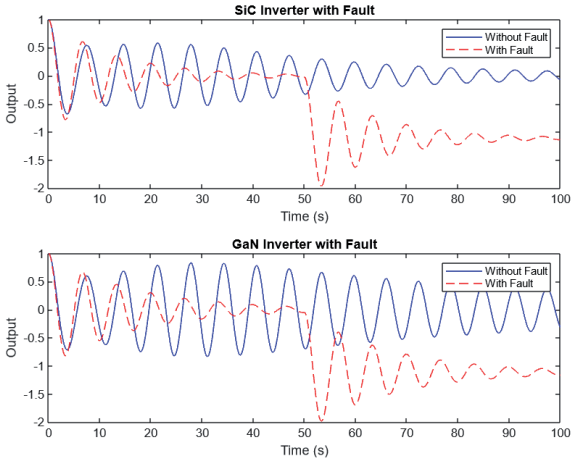

Fig. 5. Fault Tolerance Analysis for SiC & GaN Inverters, demonstrating consistent performance in faulted & non-faulted conditions. The adaptive control system effectively compensates for faults, ensuring operational stability

Algorithm 2 — Fault Introduction and Load Variation

Parameters:

$K_0 = \begin{bmatrix} 0.1 & 0.1 \end{bmatrix}$, $\gamma = 0.01$, $T = 100$, $\Delta t = 0.01$

Initializations:

$x_{\text{SiC}} = x_0$, $x_{\text{GaN}} = x_0$, $K_{\text{SiC}} = K_0$, $K_{\text{GaN}} = K_0$

for $i = 1$ **to** length(time) **do**

1. Update control actions based on error feedback:

$$u_{\text{SiC}}(i) = -K_{\text{SiC}}(i) \cdot x_{\text{SiC}}(i) + \gamma, e_{\text{SiC}}(i) \cdot x_{\text{SiC}}(i), \quad (21)$$

$$u_{\text{GaN}}(i) = -K_{\text{GaN}}(i) \cdot x_{\text{GaN}}(i) + \gamma, e_{\text{GaN}}(i) \cdot x_{\text{GaN}}(i) \quad (22)$$

where

$$e_{\text{SiC}}(i) = C \cdot x_{\text{SiC}}(i) - y_{\text{ref,SiC}}(i), \quad (23)$$

$$e_{\text{GaN}}(i) = C \cdot x_{\text{GaN}}(i) - y_{\text{ref,GaN}}(i). \quad (24)$$

2. Update state and adaptive gain matrices:

$$x_{\text{SiC}}(i+1) = x_{\text{SiC}}(i) + \dot{x}\text{SiC}(i) \cdot \Delta t, \quad (25)$$

$$x_{\text{GaN}}(i+1) = x_{\text{GaN}}(i) + \dot{x}\text{GaN}(i) \cdot \Delta t, \quad (26)$$

$$K_{\text{SiC}}(i+1) = K_{\text{SiC}}(i) - \gamma, e_{\text{SiC}}(i) x_{\text{SiC}}(i)^T \cdot \Delta t, \quad (27)$$

$$K_{\text{GaN}}(i+1) = K_{\text{GaN}}(i) - \gamma, e_{\text{GaN}}(i) x_{\text{GaN}}(i)^T \cdot \Delta t. \quad (28)$$

3. Log state trajectories and adaptive gains for dynamic response analysis:

$$\text{Log: } x_{\text{SiC}}(i), x_{\text{GaN}}(i), K_{\text{SiC}}(i), K_{\text{GaN}}(i) \quad \forall i \in [1, N] \quad (29)$$

end for

Awais Khan, Wenshou Wang, Arshad Rauf, Muhammad Ilyas, Bo Zhang, Next-Generation SiC and GaN Inverters with Advanced Real-Time Adaptive Control, Journal of Energy, vol. 74 Number 2 (2025), 13–23
https://doi.org/10.37798/2025742714

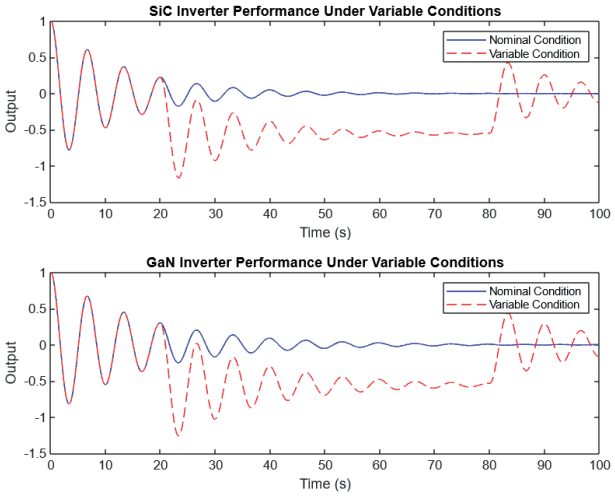

Fig. 6. Performance Under Variable Conditions for SiC and GaN inverters. Adaptive control adjusts parameters in real-time, enabling the inverters to maintain performance and reliability under load and environmental changes.

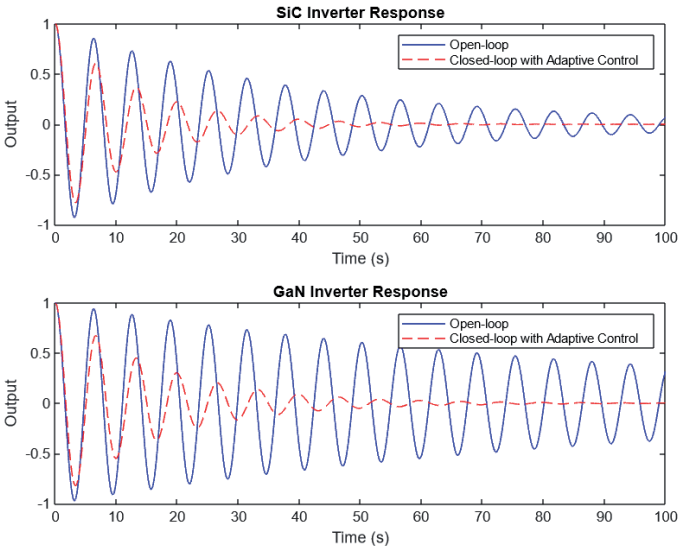

Fig. 7. Enhanced Stability through Adaptive Control for SiC and GaN inverters. The figure compares eigenvalues for closed-loop and open-loop systems, highlighting improved stability achieved with adaptive control. vehicle and renewable-energy applications.

The adaptive controller automatically compensates for this disturbance by adjusting feedback gains in real time, preventing oscillatory divergence and restoring the output trajectory within milliseconds. This behavior validates the controller's fault-resilient design, ensuring that inverter performance and output quality remain stable under partial or transient faults. In practice, such robustness minimizes downtime, protects connected systems, and enhances inverter reliability in electric-vehicle an renewable-energy applications.

Figure 6 Ilustrates the inventer's real-time adaptability under variable operating conditions. When load and enirronmental parameters change around 80 s, both SiC and GaN systems maintain smooth, stable responses without overshoot or instability. This demonstrates the controller's ability to adjust parameters online, ensuring reliable output regulation and sustained efficiency even under fluctuating operating scenarios.

Figures 7 and 8 highlight the superior stability attained through adaptive control. The closed-loop SiC and GaN inverters display rapid damping and minimal oscillations compared to their open-loop counterparts, demonstrating stronger dynamic robustness. Corresponding eigenvalue distributions positioned further left in the complex plane confirm enhancedstability margins, validating sustained efficiencies of 98.5–99% under realistic operating conditions.

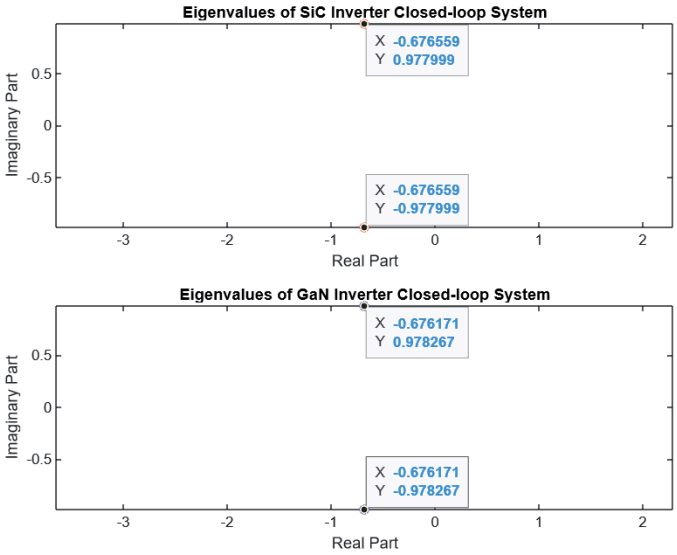

Fig. 8. Stability Analysis of Closed-Loop Systems for SiC and GaN inverters. This plot provides insights into stability improvements, with eigenvalues demonstrating enhanced control for both materials

V. Performance Analysis and Comparative Studies

To provide a comprehensive assessment of the proposed adaptive control strategy, a comparative study is conducted with other popular control techniques, including PWM, MPC and Active Thermal Control. The objective is to highlight the performance differences in terms of key metrics such as temperature stabilization, power dissipation, dynamic stability, fault tolerance, and adaptability to variable conditions. Table 1 summarizes the performance characteristics across these control methods.

The comparative analysis in Table III demonstrates that the proposed adaptive control method excels in providing efficient thermal management, stability, fault tolerance, and adaptability. Unlike PWM, which is constrained to predefined parameters and has limited fault tolerance, adaptive control dynamically adjusts its parameters in real-time, achieving rapid stabilization and resilience under various conditions. MPC shows high efficiency and adaptability due to its predictive nature; however, it is computationally intensive, which can limit its practicality in real-time applications. Active Thermal Control, while effective in thermal management, sacrifices efficiency due to energy overheads required to regulate temperature.

From a hardware implementation perspective, the proposed adaptive algorithm is computationally lightweight and can be feasibly deployed on mid-range DSPs or high-performance microcontrollers. For SiC-based inverters operating around 500 kHz, processors such as the *TI TMS320F28379D* could be utilized to provide adequate real-time computation with integrated PWM/ADC peripherals. Similarly, for GaN-based systems operating near 1 MHz, FPGA platforms such as the *Xilinx Zynq-7000* are suitable candidates to ensure deterministic execution and parallel data processing. These potential configurations indicate that the propo-

Awais Khan, Wenshou Wang, Arshad Rauf, Muhammad Ilyas, Bo Zhang, Next-Generation SiC and GaN Inverters with Advanced Real-Time Adaptive Control, Journal of Energy, vol. 74 Number 2 (2025), 13–23
https://doi.org/10.37798/2025742714

TABLE III

COMPARATIVE ANALYSIS OF CONTROL STRATEGIES FOR SIC AND GAN INVERTERS

Metric	Adaptive Control	PWM	MPC	Active Thermal Control
Temperature Profile	Efficient management with rapid stabilization around ambient 25°C (Fig. 2)	Moderate stabilization with possible overshoot	Predictive adjustment achieving efficient stabilization	Specialized for thermal control with gradual stabilization
Power Dissipation	Rapid decline to near-zero (Fig. 2)	Moderate reduction with residual loss	Optimized dissipation	Actively limits thermal rise but includes energy overhead
Dynamic Stability	Enhanced stability through real-time gain adjustment (Fig. 4)	Limited to predefined parameters	Predictive stability but computationally intensive	Moderate improvement in stability
Fault Tolerance	Effective fault compensation and recovery (Fig. 7)	Limited fault tolerance	Predictive fault handling but sensitive to model accuracy	Moderate tolerance with heat management
Adaptability to Variable Conditions	Responsive to load and environmental changes (Fig. 6)	Limited adaptability	Adaptive to predictive setpoints	Limited flexibility under thermal stress

sed control strategy is compatible with standard industrial inverter hardware, offering low latency, precise signal sampling, and robust stability for future experimental validation.

VI. CONCLUSION

This study introduces an advanced adaptive control strategy for SiC and GaN inverters, significantly enhancing efficiency, stability and fault tolerance in high-speed switching applications. Using the unique properties of WBG materials, the proposed approach outperforms conventional methods such as PWM, MPC and active thermal control, delivering superior responsiveness and energy efficiency. C omparative analyses highlight its transformative potential for next-generation inverter systems, particularly in renewable energy and electric vehicle applications demanding high reliability. Future work will include preliminary experimental validation using SiCand GaN-based inverter prototypes with a DSP platform to verify real-time control performance and stability under varying load and thermal conditions. This step will serve as the foundation for large-scale experimental implementation and practical deployment in renewable energy and electric vehicle systems. Additionally, integrating hybrid control with predictive and machine-learning techniques will address complex system dynamics, further advancing inverter technology. This research establishes a foundation for resilient, high-efficiency power electronics, accelerating the adoption of WBG materials in critical applications.

REFERENCES

[1] M. Buffolo, D. Favero, A. Marcuzzi, C. De Santi, G. Meneghesso, E. Zanoni and M. Meneghini, "Review and outlook on GaN and SiC power devices: industrial state-of-the-art, applications and perspectives," *IEEE Transactions on Electron Devices*, Jan. 2024.

[2] Z. Tong, J. Roig-Guitart, T. Neyer, J. D. Plummer and J. M. Rivas-Davila, "Origins of soft-switching Coss losses in SiC power MOSFETs and diodes for resonant converter applications," *IEEE Journal of Emerging and Selected Topics in Power Electronics*, vol. 9, no. 4, pp. 4082-4095, Oct. 2020.

[3] E. Gurpinar & A. Castellazzi, "Single-phase T-type inverter performance benchmark using Si IGBTs, SiC MOSFETs & GaN HEMTs," *IEEE Transactions on Power Electronics*, vol. 31, no. 10, pp. 7148-7160, 2015.

[4] C. Zhao, B. Trento, L. Jiang, E. A. Jones, B. Liu, Z. Zhang, D. Costinett, F. F. Wang, L. M. Tolbert, J. F. Jansen and R. Kress, "Design and implementation of a GaN-based, 100-kHz, 102-W/in³ single-phase inverter," *IEEE Journal of Emerging and Selected Topics in Power Electronics*, vol. 4, no. 3, pp. 824-840, May 2016.

[5] X. Chen, X. Yang, X. Xie, Y. Peng, L. Xiao, C. Shao, H. Li & X. Xu, "Research progress of large size SiC single crystal materials & devices," *Light: Science & Applications (Nature)*, vol. 12, no. 1, pp. 28, 2023.

[6] M. Xu, Y. R. Girish, K. P. Rakesh, P. Wu, H. M. Manukumar, S. M. Byrappa and K. Byrappa, "Recent advances and challenges in SiC ceramic nanoarchitectures and their applications," *Materials Today Communications*, vol. 28, pp. 102533, Sep. 2021.

[7] A. Abdullah, "Comparative analysis of SiC and GaN-based power converters in renewable energy systems," *National Journal of Electrical Machines & Power Conversion*, 2025, pp. 11–20.

[8] S. Pavlidis, G. Medwig, and M. Thomas, "Ultrawide-bandgap semiconductors for high-frequency devices," *IEEE Microwave Magazine*, vol. 25, no. 10, pp. 68–79, Oct. 2024.

[9] D. R. Chandran, S. Kumar, and D. Sanath, "Solid state transformers: A comprehensive review of technology, topologies, applications, research gaps, and future directions," *Journal of Power and Energy Engineering*, vol. 13, no. 6, pp. 30–64, 2025.

[10] P. Le Fevre, G. Haynes, K. K. Leong, V. Odnoblyudov, C. Basceri,` H. W. Then, *et al.*, "Challenges and future trends," in *GaN Technology: Materials, Manufacturing, Devices and Design for Power Conversion*. Cham: Springer Nature, 2024, pp. 293–351.

[11] J. P. Kozak, R. Zhang, M. Porter, Q. Song, J. Liu, B. Wang, R. Wang, W. Saito and Y. Zhang, "Stability, reliability and robustness of GaN power devices: A review," *IEEE Transactions on Power Electronics*, vol. 38, no. 7, pp. 8442-8471, Apr. 2023.

[12] J. Wei, Z. Zheng, G. Tang, H. Xu, G. Lyu, L. Zhang, J. Chen, M. Hua, S.

Awais Khan, Wenshou Wang, Arshad Rauf, Muhammad Ilyas, Bo Zhang, Next-Generation SiC and GaN Inverters with Advanced Real-Time Adaptive Control, Journal of Energy, vol. 74 Number 2 (2025), 13–23
https://doi.org/10.37798/2025742714

APPENDIX

APPENDIX A — NOMENCLATURE

TABLE IV
LIST OF SYMBOLS, PARAMETERS AND DESCRIPTIONS USED IN THE STUDY

Symbol	Description	Value / Unit
$x(t) = [i_L, v_C]^T$	State vector: inductor current and capacitor voltage	–
i_L, v_C	Inductor current, capacitor voltage	A, V
$u(t)$	Control input (duty ratio / gate drive)	–
$y(t)$	Output current (measured)	A
$y_{\text{ref}}(t)$	Reference output current	A
$A(t), B(t), C$	System matrices defining inverter dynamics	–
$A_{\text{SiC}}, B_{\text{SiC}}$	Matrices for SiC inverter	–
$A_{\text{GaN}}, B_{\text{GaN}}$	Matrices for GaN inverter	–
μ_n	Electron mobility	900 $\text{cm}^2/\text{V}\cdot\text{s}$
C_{ox}	Oxide capacitance per unit area	50 nF/cm^2
W/L	Channel width-to-length ratio	SiC: 100; GaN: 200
V_{GS}, V_{DS}, V_{th}	Gate–source, drain–source, and threshold voltages	V
λ	Channel-length modulation factor	0.01 V^{-1}
β	Transconductance constant (GaN)	0.1 A/V^2
α	Velocity-saturation coefficient (GaN)	0.5 V^{-1}
T_j, T_a	Junction and ambient temperatures	°C
R_{th}	Thermal resistance (junction–case)	SiC 0.5 °C/W; GaN 1.0 °C/W
$P_{\text{cond}}, P_{\text{sw}}$	Conduction and switching losses	W
$K(t), K_r(t)$	Adaptive feedback and feedforward gains	–
$\theta(t) = [K(t), K_r(t)]^T$	Adaptive parameter vector	–
γ	Adaptation gain constant	0.01
$\phi(t)$	Regression vector $[e(t), y_{\text{ref}}(t)]^T$	–
$e(t)$	Tracking error $y_{\text{ref}}(t) - y(t)$	–
$V_{GS,\text{nom}}, \Delta V_{GS}$	Nominal / incremental gate voltage	15 V, 5 V (SiC); 6 V (GaN)
$T_{j,\text{nom}}, T_{j,\text{max}}$	Nominal / maximum junction temperature	25 °C / 150 °C
$t_{\text{sw}}(t), t_{\text{sw},0}$	Adaptive / nominal switching interval	s
k_{EMI}	EMI compensation coefficient	0.1
$V_{DS,\text{max}}$	Maximum drain–source voltage	650 V
P, Q, Γ	Positive-definite matrices (Lyapunov analysis)	–
$V(t)$	Lyapunov function	–
$\Delta V(k)$	Discrete-time Lyapunov difference	–
ITAE	Integral of Time-weighted Absolute Error	–

Awais Khan, Wenshou Wang, Arshad Rauf, Muhammad Ilyas, Bo Zhang, Next-Generation SiC and GaN Inverters with Advanced Real-Time Adaptive Control, Journal of Energy, vol. 74 Number 2 (2025), 13–23
https://doi.org/10.37798/2025742714

Feng, T. Chen and K. J. Chen, "GaN power integration technology and its future prospects," *IEEE Transactions on Electron Devices*, 2023.

[13] J. S. Lee, R. Kwak and K. B. Lee, "Novel discontinuous PWM method for a single-phase three-level neutral point clamped inverter with efficiency improvement and harmonic reduction," *IEEE Transactions on Power Electronics*, vol. 33, no. 11, pp. 9253-9266, Jan. 2018.

[14] R. Kumar, P. Kant & B. Singh, "Modified PWM technique for a multipulse converter fed multilevel inverter based IM drive," *IEEE Trans., on Industry Applications*, vol. 57, no. 6, pp. 6592-6602, 2021.

[15] H. Esmaeili and M. Asadi, "A sliding mode controller based on robust model reference adaptive proportional-integral control for stand-alone three-phase inverter," *Journal of Modern Power Systems and Clean Energy*, vol. 9, no. 3, pp. 668-678, Jun. 2020.

[16] J. Chen, X. Du, Q. Luo, X. Zhang, P. Sun and L. Zhou, "A review of switching oscillations of wide bandgap semiconductor devices," *IEEE Transactions on Power Electronics*, vol. 35, no. 12, pp. 13182-13199, May 2020.

[17] P. Palmer, X. Zhang, E. Shelton, T. Zhang and J. Zhang, "An experimental comparison of GaN, SiC and Si switching power devices," in *IECON 2017 - 43rd Annual Conference of the IEEE Industrial Electronics Society*, Oct. 2017, pp. 780-785.

[18] A. I. Emon, A. B. Mirza, J. Kaplun, S. S. Vala and F. Luo, "A review of high-speed GaN power modules: state of the art, challenges and solutions," *IEEE Journal of Emerging and Selected Topics in Power Electronics*, vol. 11, no. 3, pp. 2707-2729, Dec. 2022.

[19] Y. Xu, X. Yuan, F. Ye, Z. Wang, Y. Zhang, M. Diab and W. Zhou, "Impact of high switching speed and high switching frequency of widebandgap motor drives on electric machines," *IEEE Access*, vol. 9, pp. 82866-82880, Jun. 2021.

[20] M. Di Paolo Emilio, *GaN and SiC Power Devices*, 2024.

[21] J. Y. Baek and K. B. Lee, "Model Predictive Current Control Strategy for Improved Dynamic Response in Cascaded H-Bridge Multilevel Inverters," *Journal of Electrical Engineering & Technology*, vol. 19, no. 3, pp. 13951405, Mar. 2024.

[22] L. Estrada, N. Vazquez, J. Vaquero, C. Hernandez, J. Arau and H. Huerta, "Finite control set–model predictive control based on sliding mode for bidirectional power inverter," *IEEE Transactions on Energy Conversion*, vol. 36, no. 4, pp. 2814-2824, Mar. 2021.

[23] Awais Khan, Wei Xie, Bo Zhang and Long-Wen Liu, "A survey of interval observers design methods & implementation for uncertain systems," *Journal of the Franklin Institute*, 358(6), pp. 3077-3126, 2021.

[24] A. R. Nair, R. Bhattarai, M. Smith and S. Kamalasadan, "A hybrid adaptive control architecture for grid-connected inverter with optimal policy generation," *IEEE Transactions on Industry Applications*, vol. 58, no. 1, pp. 855-867, Oct. 2021.

[25] J. Rabkowski, D. Peftitsis and H. P. Nee, "Silicon carbide power transistors: A new era in power electronics is initiated," *IEEE Industrial Electronics Magazine*, vol. 6, no. 2, pp. 17-26, Jun. 2012.

[26] A. Deb, "Performance and ageing mechanism of wide bandgap devices in automotive applications," Ph.D. dissertation, University of Warwick, 2024.

[27] M. Heikkinen, "Symposium A opening session," 2024.

[28] A. R. Nair, R. Bhattarai, M. Smith and S. Kamalasadan, "A hybrid adaptive control architecture for grid-connected inverter with optimal policy generation," *IEEE Transactions on Industry Applications*, vol. 58, no. 1, pp. 855-867, Oct. 2021.

[29] Z. Chen and A. Q. Huang, "Extreme high efficiency enabled by SiC power devices," *Materials Science in Semiconductor Processing*, vol. 172, pp. 108052, 2024.

[30] Y. Liu, D. Jin, S. Jiang, W. Liang, J. Peng and C. M. Lai, "An active damping control method for the LLCL filter-based SiC MOSFET gridconnected inverter in vehicle-to-grid application," *IEEE Transactions on Vehicular Technology*, vol. 68, no. 4, pp. 3411-3423, Feb. 2019.

[31] J. Millan, P. Godignon, X. Perpin˜a, A. P` erez-Tom´ as and J. Rebollo, "A´ survey of wide bandgap power semiconductor devices," *IEEE Transactions on Power Electronics*, vol. 29, no. 5, pp. 2155-2163, Jun. 2013.

[32] H. A. G. Al-Kaf, K.-B. Lee, and F. Blaabjerg, "Overview of DSP-based implementation of machine learning methods for power electronics and motor drives," *Journal of Power Electronics*, 2025, pp. 1–18.

[33] J. Huang, H. Wang, G. Gong, L. Wang, and X. Chen, "An efficient multicore DSP power management controller," *Engineering Reports*, vol. 7, no. 4, 2025, Art. no. e70079.

[34] A. Khan, F. U. Islam, A. U. Rehman, A. Rauf, M. Ilyas, "Optimized network-centric MPC using time-delay autoregressive model," *Proceedings of the Institution of Mechanical Engineers, Part C: Journal of Mechanical Engineering Science*, pp. 6091-6100, 239(15), 2025.

[35] A. Azizi, M. Akhbari, S. Danyali, Z. Tohidinejad, and M. Shirkhani, "A review on topology and control strategies of high-power inverters in large-scale photovoltaic power plants," *Heliyon*, 2025.

[36] T. Cao, Z. Ye, Q. Wu, X. Wan, J. Wang, and D. Li, "A review of adaptive control methods for grid-connected PV inverters in complex distribution systems," *Energies*, vol. 18, no. 3, p. 473, 2025.

[37] R. Wu, X. Zhang, and W. Jiang, "Bifurcation analysis and control in a DC–AC inverter with PID controller," *International Journal of Circuit Theory and Applications*, vol. 53, no. 4, pp. 2125–2153, 2025.

[38] H. Walwil, Y. Song, D. C. Shoemaker, K. Kang, T. Mirabito, J. M. Redwing, and S. Choi, "Thermophysical property measurement of GaN/SiC, GaN/AlN, and AlN/SiC epitaxial wafers using multi-frequency/spot-size time-domain thermoreflectance," *Journal of Applied Physics*, vol. 137, no. 9, 2025.

[39] P. Arevalo, D. Ochoa-Correa, and E. Villa-´ Avila, "Towards energy´ efficiency: Innovations in high-frequency converters for renewable energy systems and electric vehicles," *Vehicles*, vol. 7, no. 1, 2024.

[40] V. Anand, V. Singh, and S. Mekhlief, "Power electronics for renewable energy systems," in *Renewable Energy for Sustainable Growth Assessment*, 2022, pp. 81–117.

[41] A. Khan, U. Sarwar and B. Zhang, "Energy-Efficient MPC for SiC/GaNBased Power Electronics in Con- sumer Device," *2025 IEEE International Conference on Consumer Electronics (ICCE)*, 11-14 January 2025, Las Vegas, NV, USA.